

# Study to evaluate the abrasive wear resistant behavior of materials coated with Fe-Cr-Si-C

M. Yaz<sup>1\*</sup>, S. O. Yılmaz<sup>2</sup>, T. Teker<sup>3</sup>

<sup>1</sup>Firat University, Vocational High School of Technical Sciences, Elazig-23119, Turkey

<sup>2</sup>Firat University, Material and Metallurgical Engineering Faculty, Elazig-23119, Turkey

<sup>3</sup>Firat University, Technical Education Faculty, Metal Department, Elazig-23119, Turkey

Received 14 August 2009, received in revised form 25 November 2010, accepted 11 February 2011

## Abstract

Surfaces that are coated with steel are considered useful for grinding and milling applications based on their ability to resist abrasions. In the present study, the microstructures of hypoeutectic, eutectic, and hypereutectic compositions in 10–20 wt.% chromium (Cr) samples were studied with respect to the micro-structural transitions of the coatings and several other processing parameters. In addition, tests were conducted in order to analyze the influence of the microstructure of the coated surfaces on the capacity of the hypoeutectic, eutectic, and hypereutectic Cr-enriched microstructures of the samples coated with 10–20 wt.% Cr alloy to resist wear. Consequently, it was found that based on the presence of an austenitic matrix within them, the coated regions effectively resisted abrasions.

**Key words:** coating, gas tungsten arc welding (GTAW), surface modification, chromium

## 1. Introduction

It is known that the materials that possess a high concentration of chromium (Cr), constituted in Cr-rich carbides, are used for various applications, wherein the ability to remain stable in an aggressive environment is the principal requirement. Some of these applications are mining and mineral processing, cement production, and pulp and paper manufacturing industries. These chromium-rich materials are alloys or surfaces that possess a superior power of abrasive wear resistance, along with relatively low production costs. Based on these two properties, these alloys are preferred for applications, wherein hard materials, such as ores, coal, gravel, and cement are processed by the grinding, milling, and pumping apparatuses. The exceptional abrasive wear resistance power of the alloys can be related to the high volume of hard carbides present in them; however, the toughness of the matrix also contributes significantly to the degree of wear resistance [1–4]. The surfaces coated with 10–30 wt.% Cr along with 2.5–4.0 wt.% carbon (C) can also be described as composites containing large, hard proeutectic, and/or eutectic  $M_7C_3$  carbides within a

softer iron matrix. The matrix structure that constitutes 10–30 wt.% Cr along with 2.5–4.0 wt.% C is most often considered to be an austenite. The carbides that are present in the structure of these alloys are typically of the  $M_7C_3$  type (wherein  $M = Fe, Cr$ ). The  $M_7C_3$  carbides eventually grow as rods and blades, in a direction such that their long axes are parallel to the direction of heat flow. On the other hand, the microstructure of these surfaces must also be well characterized after being coated, because the wear-resistant surfaces are typically used in surfaces coated with thin layers of alloys [5]. Some investigations revealed the effects of conducting a process of solidification on the microstructure that contained 10 wt.% Cr alloys [6–9] and studied the relationship between the structure and the toughness of the fracture.

In recent years, the in-situ synthesis of the  $M_7C_3$  carbide that reinforced existing composite surfaces in the metal matrix, which were produced by subjecting a liquid FeCrC ferro-alloy to the process of high temperature synthesis, and the surface alloy to the gas tungsten arc welding (GTAW), and the plasma and laser beam techniques generated much interest world-wide [10–15]. These techniques revealed that the

\*Corresponding author: tel.: +90 424 237 00 00/4407; fax: +90 424 2188947; e-mail address: [myaz@firat.edu.tr](mailto:myaz@firat.edu.tr)

Table 1. Effect of processing parameters on the coating geometry and microhardness

Sample Structure	Process parameters						Coating dimensions ( $\mu\text{m}$ )				Microhardness
	Power (kW)	Electrode diameter (mm)	Process speed ( $\text{mm s}^{-1}$ )	Powder feed rate ( $\text{g s}^{-1}$ )	Power density ( $\text{kW cm}^{-2}$ )	Specific energy ( $\text{J cm}^{-2}$ )	$d_c$	$h_c$	$t_c$	$w_c$	HV
S <sub>1</sub> Hypoeutectic	5	3.2	6.5	0.2	45	22.3	1200	700	1900	9700	512
S <sub>2</sub> Eutectic	3	3.2	10	0.3	24	11.1	110	1600	1710	8150	798
S <sub>3</sub> Hypereutectic	2	2.4	25	0.5	16	7	25	1140	1165	6600	807
S <sub>4</sub> Hypoeutectic	5	3.2	6.5	1	95	10.8	250	1320	1570	2300	835
S <sub>5</sub> Eutectic	3	2.4	10	1.2	45	6.8	680	1560	2240	7100	845
S <sub>6</sub> Hypereutectic	3	2.4	25	1.7	24	4.2	10	4930	4950	9125	973

$d_c$  – max depth below the original substrate surface,  $h_c$  – max height above the original substrate surface,  $t_c$  – max total thickness ( $d_c + h_c$ ),  $w_c$  – max width, HV – average of three measurement

interfacial incompatibility of matrices was eliminated by creating more thermodynamically stable reinforcements based on their nucleation and growth from the matrix phase of the parent [16].

Some studies in the past also revealed that a tungsten inert gas heat source had the potential to be effectively used for carrying out surface modification [17, 18]. However, in this GTAW method, too, some problems do persist owing to the roughness and thickness of the surface of the heat affected zone [14]. On the other hand, the plasma and laser beam method is quite expensive and difficult in comparison with the complex components entailed in the GTAW method [14, 15]. Recently, the GTAW melting process has been widely employed to achieve surface composite coatings, wherein the alloying powders were externally fed to a melting bath and a thin surface layer was simultaneously melted and then solidified [17]. The wear-resistant behavior of a coating highly enriched with Cr is a function of its chemical composition as well as the conditions entailed in the processing procedure; therefore, each coated surface must be evaluated with respect to these variables, as well as the related tribological environment [10–17]. The important microstructural parameters that are considered significant in influencing the ability of the coating material to resist wear-resistance include the quantity, orientation, and morphology of the carbides present in them [15–20], the kind of matrix found within them [20], and the overall structure of the coatings [15, 16]. Additionally, the abrasive wear-resistant behavior of the coated surface also depends on the characteristics of the tribological environment, such as the kind of abrasive involved, the relative movement of the wear surface, the loading conditions, the existence of an aggressive chemical species, and the relative temperature of the triboenvironment [12, 13].

The method of GTAW processing was employed to coat a metal by creating an electric arc between a tungsten electrode and the base metal. This arc re-

gion was protected by the argon inert gas. For this experiment, the electrode was heated to temperatures that were high enough to emit electrons required by the arc to operate effectively. Along with conducting these evaluations, the aim of this present study was to first establish relationships between the chemical composition and the solidification temperatures of the samples constituting 15 and 26 wt.% Cr by means of the gas tungsten arc processing. Its second objective was to detect the effect of the macrostructure and microstructure of the coated regions on their wear-resistant ability under abrasive conditions.

## 2. Experimental procedure

For the purpose of conducting the GTAW processing experiments, rectangular plates of low carbon steel (AISI 1018, 12.7 cm long, 5.1 cm wide and 0.9 cm thick) were employed as substrates. A powder mixture containing iron (Fe), chromium (Cr), silica (Si), and carbon (C) in a weight ratio of 3 : 10 : 0.5 : 1 was used as the coating alloy powder. The experimental conditions followed herein are listed in Table 1. The chemical compositions of the three different microstructures of the coated surfaces for 10 and 20 wt.% Cr were obtained through the EDS analysis, and are listed in Table 2. It was noted that the carbon levels of both compositional series varied slightly, as was reflected by the hypoeutectic, eutectic, and hypereutectic compositions.

Further, an electronic power supply was generated through a mechanized system and the test piece was moved at a variable speed under a GTA torch to eventually produce bead-on-plate coatings. In order to examine the effect of the processing parameters on the microstructure, microchemistry, and the properties of the GTA-processed coatings, the measures of the entailed parameters were varied as follows: the value of power ( $P$ ) was altered from 2 to 5 kW, the value of

Table 2. Chemical composition (wt.%) and density ( $\text{g cm}^{-3}$ ) of the coated surfaces

Sample	Structure	Cr	C	Si	Fe	Density
S <sub>1</sub>	Hypoeutectic	10.3	3.51	1.1	Balance	7.42
S <sub>2</sub>	Eutectic	10.2	3.75	1.12	Balance	7.52
S <sub>3</sub>	Hypereutectic	10.1	4.41	1.05	Balance	7.6
S <sub>4</sub>	Hypoeutectic	20.3	2.77	0.98	Balance	7.52
S <sub>5</sub>	Eutectic	20.1	3.11	0.96	Balance	7.54
S <sub>6</sub>	Hypereutectic	20.2	3.68	0.91	Balance	7.58

process speed ( $V$ ) from 6.5 to 25  $\text{mm s}^{-1}$ , and the rate of the powder feed ( $f$ ) from 0.05 to 1.5  $\text{g s}^{-1}$ . The diameter of the electrode ( $d$ ) used in all the experiments was 2.4 and 3.2 mm. Further, in order to facilitate a relatively inert environment during the experiment, the GTAW processed surfaces were covered by argon gas at a rate of (10  $\text{l min}^{-1}$ ) that flew over the processing region. The chemical composition of the coated surfaces was determined through X-ray wavelength dispersive spectrometry, whereas their carbon content was measured by a combustion infrared detection technique. The average carbide size and volume fraction were determined through the quantitative metallography technique by using a digital image analyzer.

The differential thermal analysis (DTA) was performed by mounting an instrument constituting a pair of matched alumina crucibles with tantalum lids. One of the crucibles contained the sample of a mass of between 50 and 100 mg, while the other crucible was kept empty. The samples that were subjected to DTA were cut in a similar way as the metallographic specimens were incised from the coated surfaces. After evacuating the DTA chamber, a flow of 1.67  $\text{cm}^3 \text{s}^{-1}$  of argon of high purity was maintained throughout the experiment. The specimens were heated at a rate of 5  $^{\circ}\text{C min}^{-1}$  to 700  $^{\circ}\text{C}$ , which was approximately 50  $^{\circ}\text{C}$  above their normal liquid temperature. A cooling rate of 5  $^{\circ}\text{C min}^{-1}$  was considered as the average cooling rate in the DTA experiments. The temperature difference between the crucibles was monitored during both the heating and the cooling processes. The consequent heat absorbed or emitted during the analysis was plotted after normalizing the temperature of the sample weight.

Additionally, the dry abrasive wear resistant tests were conducted by using a pin-on-disc type of apparatus at room temperature. However, before initiating the wear tests, each specimen was ground up to an abrasive paper of grade 1200, ensuring that the wear surface was in complete contact with the surface of the abrasive paper. The abrasive wear-resistant tests were carried out under various loads of 20, 80, and 140 N on a grade 80 SiC abrasive grinding disk, which rotated at a sliding speed of 3000  $\text{m h}^{-1}$ , along a sliding distance of 100 m and an abrading duration of 60 s. Each individual test was performed at least three times. The

rate of wear was obtained by determining the masses of the samples prior to and subsequent to conducting the wear-resistant tests.

Moreover, the microhardness measurements were calculated from the cross-section area of the coated surface to substrates. For ascertaining these measurements, the microhardness indentations in the coated surface were made with a load of 50 g. The varied values of the microhardness of the coatings of different structures are listed in Table 1.

The specimens that were subjected to a microstructural characterization were prepared by first dividing the coatings into sections in the transverse and longitudinal directions and then polishing them sequentially with 240, 320, 400, 600, grit SiC, 0.3  $\mu\text{m}$   $\alpha\text{-Al}_2\text{O}_3$ , and 0.05  $\mu\text{m}$   $\gamma\text{-Al}_2\text{O}_3$ . The microstructures of the samples were revealed by a solution that contained 5 g of  $\text{FeCl}_3$ , 30 ml of HCl, and 100 ml of distilled water. The XRD analyses were conducted by means of a Rigaku Geigerflex X-ray diffractometer that was operated at 40 kV and 30 mA by employing the Mo  $\text{K}\alpha$  radiation. The microstructures were characterized by means of both optical microscopy (OM) and scanning electron microscopy (SEM). This present study, however, focused on evaluating the microstructures present in the molten pool.

### 3. Results

#### 3.1. Microhardness

The diameter of the electrode and the speed of the alloying process were considered for investigating the coating geometry and the characteristic of hardness of the samples at lower degrees of specific energies. A comparison of the samples revealed that for relatively low rates of process speeds and equivalent rates of powder feed, a significant increase in the powder density promoted the formation of thicker and harder coatings and melted regions below the original surface with negligible thickness. The results obtained from evaluating the microhardness of the coating for each sample are listed in Table 1. In addition, the data in Table 1 also reveal that for a high rate of power density, when the rate of process speed is increased (or

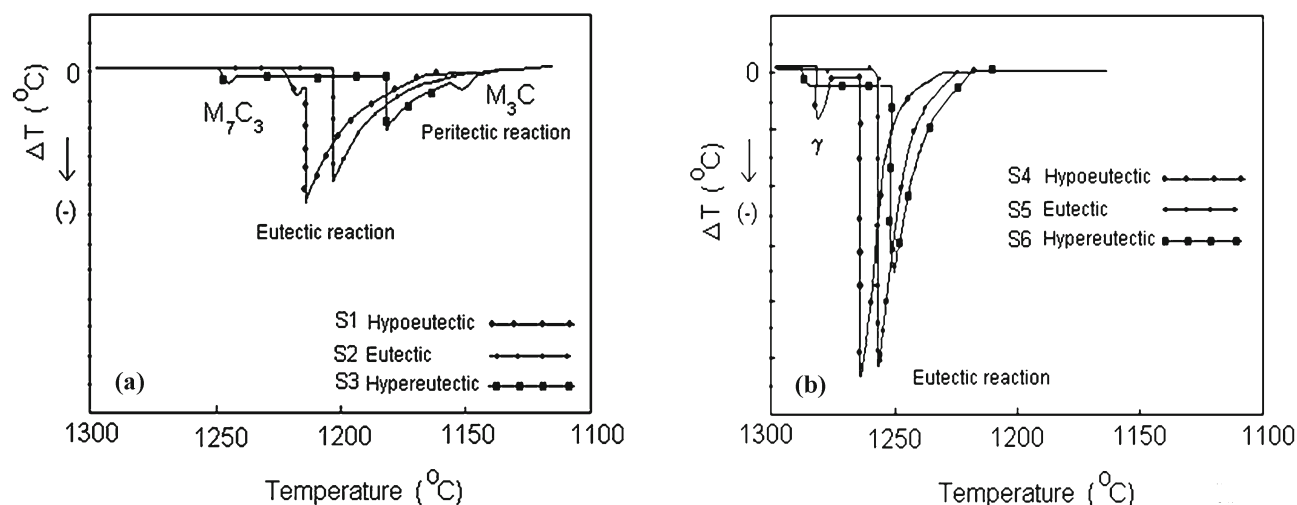


Fig. 1. The DTA curves of hypoeutectic, eutectic, and hypereutectic regions of (a) samples having 10 wt.% Cr and (b) samples having 20 wt.% Cr.

the degree of specific energy is reduced), the thickness of the coating significantly reduces without appreciably affecting its degree of hardness. The trends of the coating dimension and the hardness with increasing rates of powder feed and process speed were found to be similar to the samples that were obtained with an electrode diameter of 2.4 as well as 3.2 mm. Based on the parameters entailed in the process, the hardness of the coated regions assumed values in the range of 500 to 1000 HV. The results given in Table 1 illustrate the role played by the parameters entailed in the gas tungsten arc processing on the resulting dimensions, the hardness of the coating, and the extent of intermixing with the substrate material across the interface. The samples that contained 20 wt.% Cr tended to be slightly harder than the samples containing 10 wt.% Cr. The rate of hardness was recorded to increase with an increase in the carbon level for a given amount of chromium. The rate of increase in the hardness was greater for the samples that contained a high content of chromium.

### 3.2. Thermal analysis

The DTA results obtained for the coated surfaces of the samples that contained 10 wt.% and 20 wt.% Cr are illustrated in Fig. 1. It is seen that all reactions in the three samples that contained 10 wt.% Cr occurred at lower temperatures in comparison with similar reactions that occurred in the samples that contained 20 wt.% Cr.

Figure 1a shows wider reaction peaks, which reveal the amount of energy released during phase transformation, whereas the eutectic reactions illustrated in Fig. 1b occur at a much faster rate than that evident for sample S<sub>1</sub>. The hypereutectic microstructure of sample S<sub>3</sub> solidifies first with the formation of the

proeutectic  $M_7C_3$  carbides. The measure of the areas existing under the DTA curve in Fig. 1b represents the enthalpy of formation of the phases, and the wide-ness of the peaks provides information regarding the formation temperature and range of the phases [15]. Additionally, the  $M_7C_3$  peaks in the two figures are small and wide, due to the temperature of 1200°C entailed in the eutectic reactions illustrated in Fig. 1a and that of 1256°C in Fig. 1b. This means that  $M_7C_3$  was produced from the melt at a relatively slow rate. On the other hand, proeutectic austenite was first created in the hypoeutectic microstructures, followed by the monovariant eutectic reaction ( $L \rightarrow \gamma + M_7C_3$ ). As is evident from the figures, the austenite reaction was initiated at comparatively higher temperatures in Fig. 1b than in Fig. 1a. Moreover, it was seen that the measures of the areas existing under the DTA curves in Fig. 1a were in a smaller range than those found in Fig. 1b. The values of Fe and Cr content in the  $M_7C_3$  and the matrix were also noted to be quite different for both the sample groups. It was recorded that in the samples constituted with 20 wt.% Cr, the  $M_7C_3$  phase contained a larger content of Cr than in the samples that were constituted with 10 wt.% Cr, whereas, the austenite phase revealed the presence of a larger amount of Cr and a small one of C. The free energy of formation of  $M_7C_3$  increased with an increase in the Cr content of the carbide at 1000°C [2, 21]. This increase in the amount of formation energy was probably based on the difference that arose in the values of Cr content. An increase in the carbon content decreased the initial temperature of the eutectic reaction. In the samples interpreted in Fig. 1a, additional heat was evolved due to the occurrence of a peritectic reaction subsequent to the eutectic reaction. This is termed as the invariant peritectic reaction ( $L \rightarrow M_7C_3 \rightarrow M_3C$ ). However, two more reactions occur subsequent to the

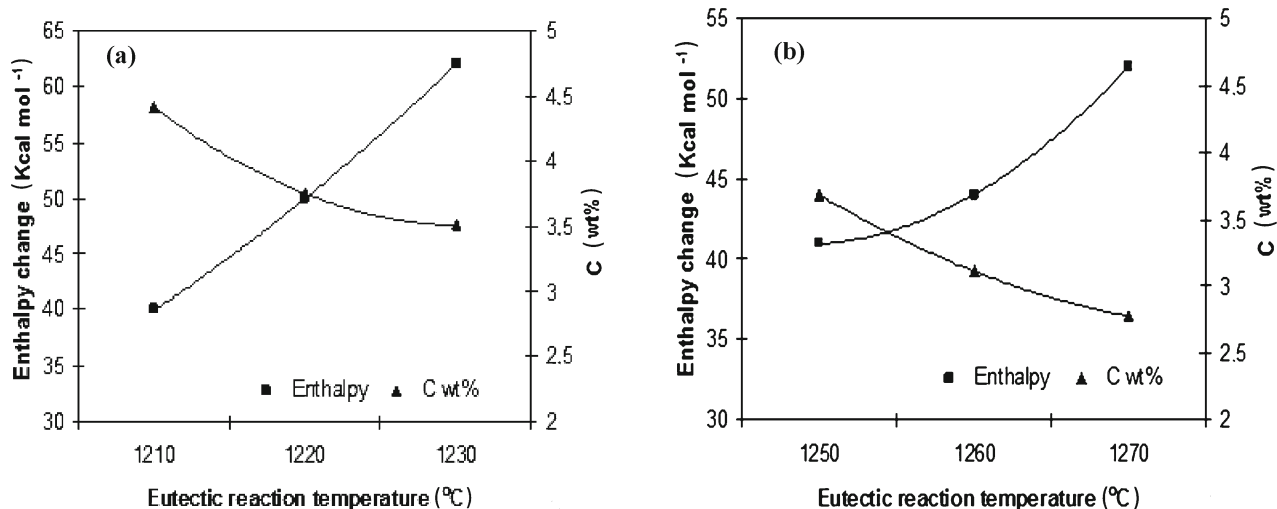


Fig. 2. The relationship between enthalpy change, eutectic reaction temperature and C wt.% for (a) sample having 10 wt.% Cr, (b) sample having 20 wt.% Cr.

occurrence of the peritectic reaction:  $(L \rightarrow \gamma + M_3C)$ , and the binary Fe-C eutectic reaction  $(L \rightarrow \gamma + Fe_3C)$ , which occurs at about 1143°C. However, it was noted that the latter reaction mentioned above did not occur at lower levels of carbon in samples that contained 10 wt.% Cr, since the samples  $S_1$ ,  $S_2$ , and  $S_3$  solidified at temperature much before this one. The reaction peaks in Fig. 1a are recorded to follow a slower rate in comparison with equivalent reactions that occur in Fig. 1b. The change in the level of the enthalpy of the eutectic reaction is given in Fig. 2. It is quite evident that the value of enthalpy change of the eutectic reaction of the samples containing 10 and 20 wt.% Cr increased, and the wt.% C of the samples decreased as a function of the entailed temperature. It is known that the wt.% C of the coated surface influences the temperature of the eutectic reaction in a way such that a decrease in the C wt.% value increases the eutectic temperature. It was also recorded that the change in the C wt.% value and the rate of change of the enthalpies altered in converse directions [21]. This difference that arose between the rate of change of enthalpy and the C wt.% value of the two groups was considered to be based on the kind of carbide used herein and its morphology. Additionally, it was also considered that for the sample that constituted 10 wt.% Cr, both the reactions (eutectic and peritectic) took place; hence the rate of potential energy decreased during the eutectic reaction. Finally, it was ascertained that the rate of solidification of the eutectic reaction was increased by increasing the Cr content.

### 3.3. Microstructure

The microstructure of the coated surface varied significantly in terms of both chemical composition and the value of power density for the sample contain-

ing 10 wt.% Cr as well as the one containing 20 wt.% Cr. Figure 3 illustrates this variation for the samples  $S_1$ ,  $S_2$ , and  $S_3$ ; whereas Fig. 4 shows the microstructure of the samples  $S_4$ ,  $S_5$ , and  $S_6$ . It is evident from both Figs. 3 and 4 that the high degree of power density resulted in forming a completely columnar structure therein. The hypoeutectic and eutectic microstructures contained quite similar volume fractions of the columnar and the equiaxed grains. On the other hand, the structure that was present in the hypereutectic compositions was recorded to be composed of just the equiaxed grains. The primary carbides, which were created first during the hypereutectic regions of the solidification process in the hypereutectic regions, were considered to be the more effective nuclei for the eutectic phase than the proeutectic austenite dendrites of the hypoeutectic microstructures. The samples  $S_3$ ,  $S_4$ , and  $S_5$ , which contained higher amounts of chromium, were recorded to be composed of the austenitic matrix and just  $M_7C_3$  carbides, with no notable presence of any other kind of carbides (Fig. 4a,b,c). Additionally, the  $M_7C_3$  carbide was found to be produced along with the austenite during the occurrence of the eutectic reaction [21]. The sample  $S_4$  contained proeutectic austenite dendrites and eutectic cells, which were composed of the  $M_7C_3$  carbides. The austenite dendrites were recorded to be finer in size in the low-power feed (deep regions) than in the regions of high power feed. The microstructure of the sample  $S_5$  (Fig. 4b) was found to be composed completely of austenite and the  $M_7C_3$  carbides. The carbide size found here was the finest in the eutectic regions and its structure was similar to that of a rod. Moreover, the  $M_7C_3$  carbides were found to be very fine at the center of the eutectic cells, and then became coarser with an increase in the distance from the center of the molten pool. In the sample  $S_6$  that contained hyper-

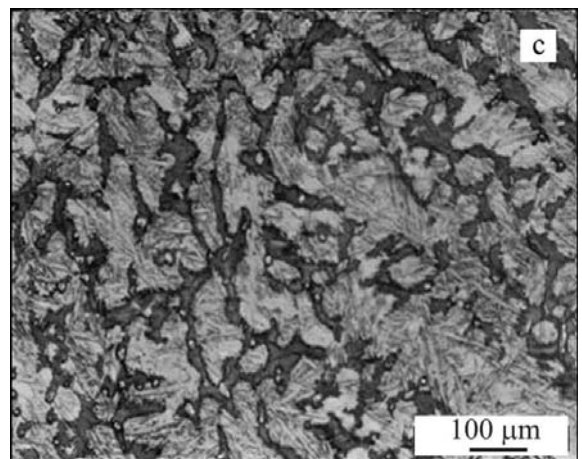
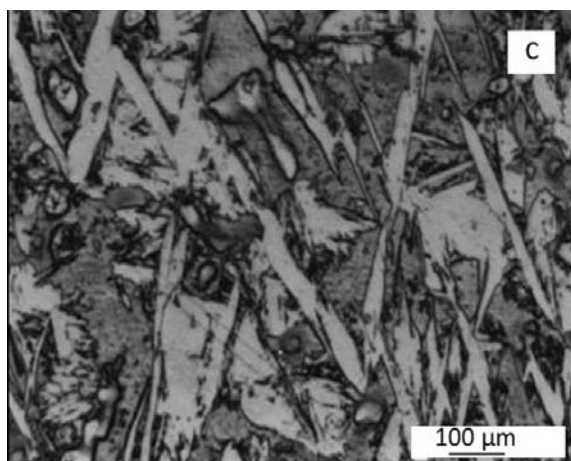
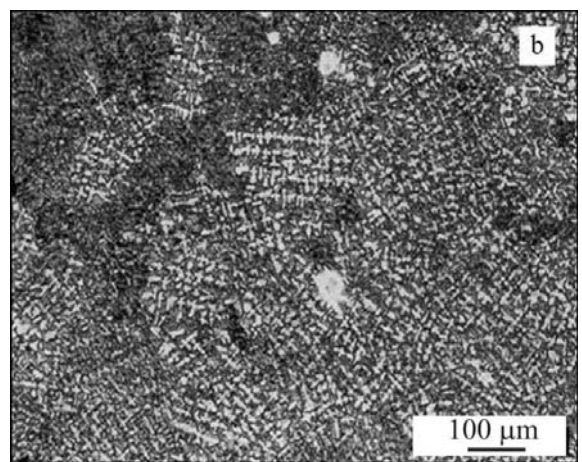
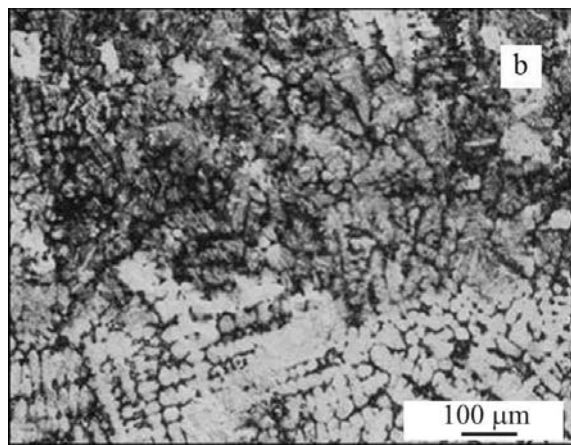
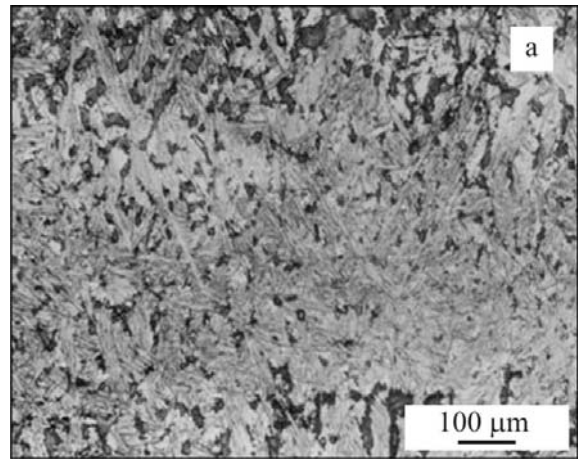
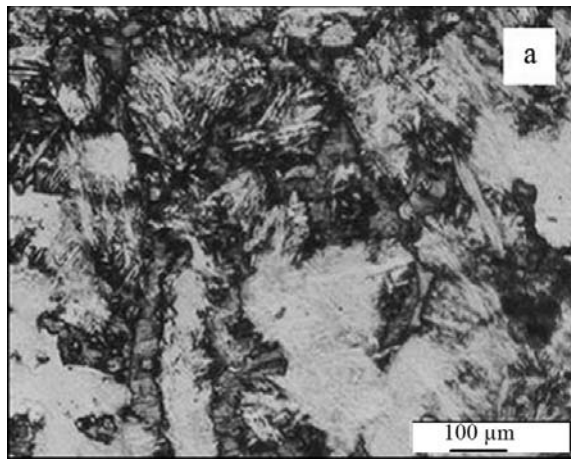


Fig. 3. Microstructure of the samples (a) S<sub>1</sub>, (b) S<sub>2</sub>, (c) S<sub>3</sub>.

Fig. 4. Microstructure of the samples (a) S<sub>4</sub>, (b) S<sub>5</sub>, (c) S<sub>6</sub>.

eutectic microstructures (Fig. 4c), large proeutectic  $M_7C_3$  carbides were formed with the eutectic cells ( $\gamma$  and  $M_7C_3$ ). The blade-shaped carbides found in the eutectic cells appeared to be located around the proeutectic  $M_7C_3$  carbides.

The chemical compositions of the samples obtained by the EDS analysis are listed in Table 2. It is observed that the carbide found in all these regions is primarily

of the  $M_7C_3$  type. It is also seen that the Fe/Cr ratio of the atomic fractions in the  $M_7C_3$  carbides of the S<sub>1</sub> and S<sub>2</sub> was approximately 1.1, whereas its value in S<sub>3</sub> was 1.37. On the other hand, the carbides present in the samples with 20 wt.% Cr contained a larger amount of Cr than of Fe. The Fe/Cr ratio of the  $M_7C_3$  carbides was found to be 0.41 in the S<sub>4</sub> sample and 0.52 in the S<sub>5</sub> and S<sub>6</sub> samples. The volume fractions of

Table 3. Volume fraction and size of primary carbides in each sample

Sample	Structure	Volume fraction of carbides (Image analysis)	Average carbide particle diameter ( $\mu\text{m}$ )
S <sub>1</sub>	Hypoeutectic	0.33	4.8
S <sub>2</sub>	Eutectic	0.36	2.8
S <sub>3</sub>	Hypereutectic	0.47	5.3
S <sub>4</sub>	Hypoeutectic	0.27	4.9
S <sub>5</sub>	Eutectic	0.31	4.2
S <sub>6</sub>	Hypereutectic	0.42	7.4

the carbides present in these samples were obtained by means of a Leica Q550 digital image analyzer mounted with a microprocessor, and the results are listed in Table 3. The carbide volume fraction increases with an increase in the contents of carbon and chromium. The samples that contain a higher input of heat revealed the presence of carbide of large sizes. For a given degree of specific energy, the eutectic samples are recorded to contain carbide of the finest average size, while the samples of hypereutectic contain the coarsest carbides.

The chromium content of the matrix of the chromium alloyed steel surfaces decreases with an increase in the carbon content [14]. A decrease in the chromium content of the matrix has two important effects. The chromium depresses the temperature of the martensitic transformation [25], since a higher level of chromium makes the matrix to remain austenitic. Once the  $\text{M}_7\text{C}_3$  precipitates were formed in the hypereutectic structure, the decreasing solidification temperature of the molten pool may not be sufficient to completely dissolve the  $\text{M}_7\text{C}_3$  carbides. The  $\text{M}_7\text{C}_3$  particles in the melt may act as nucleation sites for the equiaxed grains in the subsequent eutectic solidification process. The ease of austenite nucleation was strongly dependent upon the composition of the melt. Austenite was considered to be the primary phase to be formed in the hypoeutectic samples. However, this austenite phase was not considered to be an efficient nucleus for the eutectic phase. The equiaxed zone was approximately of the same size in both the hypoeutectic and eutectic samples. In the eutectic samples, it was impossible to follow a similar nucleation process to produce an equiaxed structure, since in this case, only one reaction took place during the solidification process. The carbides present in these samples probably reflected rod or blade morphologies. The samples S<sub>2</sub> and S<sub>5</sub> contained rod-shaped  $\text{M}_7\text{C}_3$  carbides only, whereas the samples constituting hypoeutectic and hypereutectic structures contained both rod- and blade-shaped carbides. In the white cast irons that contain large amounts of chromium of hypereutectic structures, the proeutectic  $\text{M}_7\text{C}_3$  carbides were recorded to be always rod-shaped, and conducting a subsequent process of solidification around the proeutectic carbides resulted in the formation of

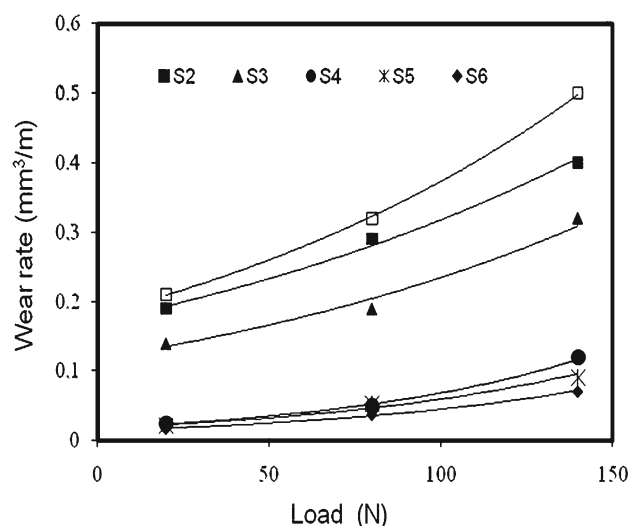


Fig. 5. The effect of load on wear rate of samples.

blade-shaped carbides [21]. This morphology suggests that during the process of alloying carried out by the GTAW method, the level of under cooling was found to be high at the surface and decreased toward the subsurface. Hence from the surface to the steel, the decrease of the level of under cooling favored the blade-like shape of carbide formed due to the heat released by the formation of the proeutectic  $\text{M}_7\text{C}_3$  carbides.

### 3.4. Wear tests

The relationship that exists between the rate of volume of wear and the load for each sample is illustrated in Fig. 5. The hypereutectic samples (S<sub>3</sub>, S<sub>6</sub>) possess the lowest wear rate in each group, whereas the hypoeutectic samples (S<sub>1</sub>, S<sub>4</sub>) reflect the highest wear rate among all. The samples constituting 20 wt.% Cr (S<sub>4</sub>, S<sub>5</sub>, and S<sub>6</sub>) reflect a lower volume of wear rate than the samples that constitute 10 wt.% Cr (S<sub>1</sub>, S<sub>2</sub>, and S<sub>3</sub>). The sample S<sub>4</sub> which contains hypoeutectic microstructures demonstrates a lower degree of wear rate than the sample S<sub>3</sub>. The rate of energy feed is also known to have a significant effect on the hardness of the coated surfaces due to the influence of the un-

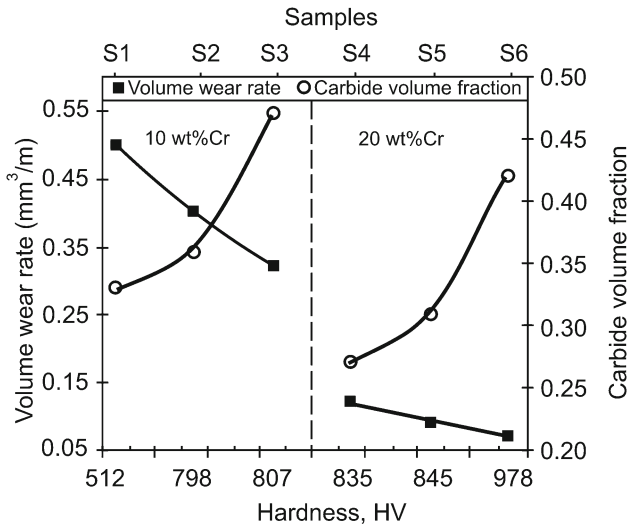


Fig. 6. The change of wear rate with hardness, carbide volume rate for samples.

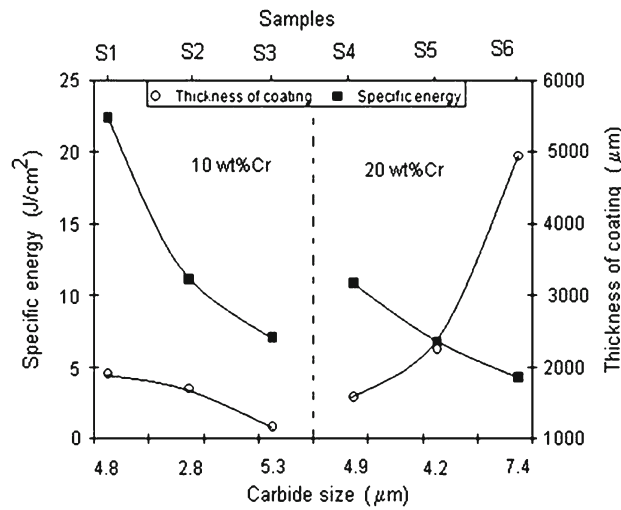


Fig. 7. The effect of specific energy on carbide size and coating thickness of samples.

der cooling on the carbide morphology, regardless of its composition.

The relationship that exists between the rates of hardness-wear and those of carbide volume is given in Fig. 6. It is recorded that the degree of wear rate decreased with an increase in the carbide volume fraction, and in the degree of hardness. The relationship that exists between specific energy, the size of the carbides, and the thickness of the coating, is illustrated in Fig. 7. It is recorded that with an increase in the degree of specific energy, the thickness of the coating increased, whereas, the size of the carbide decreased.

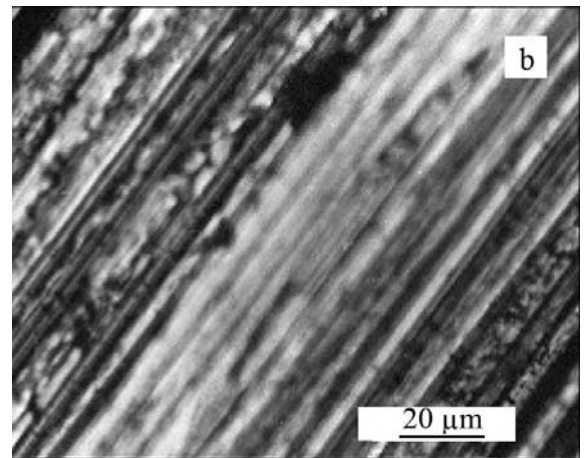
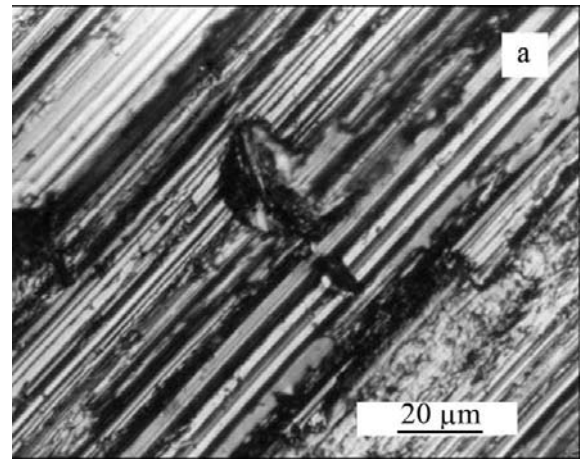


Fig. 8. The wear surfaces of the samples (a) S<sub>3</sub>, (b) S<sub>6</sub>.

The worn surfaces of the specimens subjected to the wear test revealed a significantly higher level of damage in the samples containing 10 wt.% Cr (Fig. 8a) than the samples containing 20 wt.% Cr (Fig. 8b). The wear grooves formed at the surface of the S<sub>3</sub> appeared to be deeper than in S<sub>6</sub>. The piled-up material found along the edges of the grooves on the wear surfaces of S<sub>6</sub> was not smooth and any signs of cracking were not obvious in the S<sub>3</sub>. However, the cracks caused by interactions with the abrasive environment were found to be present in the carbides. Although these cracks were observed in all the specimens, yet they were most common in the samples that contained lower concentrations of chromium. The large proeutectic carbides were found to be tougher than the eutectic carbides and therefore they did not fracture as easily [25]. As a result, the larger carbide particles were recorded to be more resistant to damage, and hence, more effective in protecting the softer matrix from damage caused by the abrasive particles [25]. The matrix was found to be austenite in the samples containing 20 wt.% Cr (S<sub>4</sub>, S<sub>5</sub>, and S<sub>6</sub>), and pearlitic/bainitic combination in

the samples containing 10 wt.% Cr ( $S_1$ ,  $S_2$ , and  $S_3$ ). Austenite is known to transform into a harder, more wear-resistant martensite under a highly stressed environment [26]. In Fig. 9, the results obtained by the X-ray diffraction analyses show the change that occurs in the phases on the wear surface of the sample  $S_4$ . Figure 9a shows the presence of the austenite, martensite, and  $M_7C_3$  phases on the unworn surfaces. On the other hand, Fig. 9b indicates that this particular specimen did not contain any significant austenite in the abraded surface. The matrix of the Cr concentration present in the samples exhibits different behaviors depending on various factors. The primary difference that exists among the samples was found to be the extent of plastic deformation caused in the piled-up regions that lay adjacent to the formed groove. However, the matrix was found to be extensively fractured in the samples that contained low levels of chromium. Moreover, it was recorded that the region around the carbides in each material was cut and chipped. The wear results indicate the importance of the impact of the matrix and the carbide volume fraction on the wear behavior. A decrease in the wear rate with an increase in the carbide volume fraction demonstrates that this decrease in the wear rate could be obtained by producing a structure that constitutes an austenitic matrix rather than a pearlitic/bainitic one. The austenitic sample had a relatively low carbide volume fraction but their volume wear rate was found to be half of that of the pearlitic/bainitic alloy. The presence of austenite in surfaces that are highly enriched in chromium causes several properties that make the austenitic composition more abrasion resistant under the experimental conditions. Ductility, strain hardenability, and thermodynamic metastability at room temperature are some of its important properties [27]. The plastic deformation allowed the matrix to dissipate the mechanical energy introduced by each abrasive particle into a larger volume; hence, the damage caused per unit volume was quite less. In contrast, the mechanical energy was dissipated into a much smaller volume in the pearlitic/bainitic samples, because the pearlite and bainite phases were less ductile [27, 28]. Moreover, the process of strain hardening may have probably occurred in the austenitic matrix as a result of the plastic deformation caused by the abrasive particles. Thus, the degree of hardness of the matrix increased, leading to a lower wear rate [15, 29]. The austenite matrix could possibly support the carbides after they were fractured by reducing the rate of material removal. The third property that increased the degree of wear resistance of the samples at room temperature is the capacity of the austenite phase to become metastable. The plastic deformation of the matrix at the wear surface led to a strain-induced transformation of the austenite to martensite [9, 30, 31]. The martensitic layer that was removed by the abra-

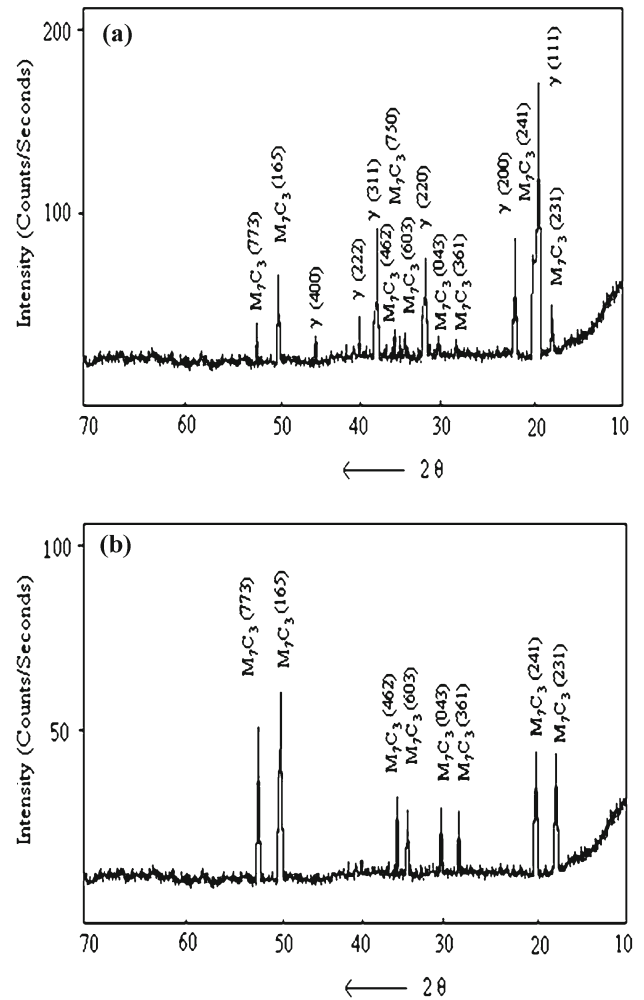


Fig. 9. X-ray diffraction spectra taken from the surface of the  $S_4$  (a) before and (b) after abrasion test.

sion followed a subsequent process as the exposition of the underlying austenite to strain by the abrasive process. A portion of the mechanical energy of the triboenvironment was employed in phase transformation rather than in debris generation during the abrasion process. Furthermore, subsequent wear requires micro plowing, micro cracking, and micro cutting of the harder, strain-induced martensitic surface [14]. In comparison, the wear process of the hard matrix in the samples constituting 10 wt.% Cr involved only limited micro plowing. The wear behavior occurred differently as a function of the carbide arrangement in the matrix [15]. It was recorded that as the carbides became thicker, the fracture became more difficult. The surfaces that possessed high level of chromium contained either low inputs of heat or hypereutectic compositions that constituted larger carbides, and were expected to be more resistant to abrasion.

#### 4. Conclusion

1. The columnar microstructures were obtained at low inputs of heat. The samples constituting hypoeutectic and eutectic compositions possessed both columnar and equiaxed zones along with a high degree of heat input. On the other hand, the hypereutectic samples were formed in an equiaxed macrostructure with a low heat input, since the proeutectic  $M_7C_3$  carbides were formed at higher temperatures than the rest of the microstructure and therefore, upon heating dissolved quite slowly into the melt.

2. The equiaxed microstructure led to induce lower wear rates than a columnar macrostructure. This effect was recorded to be more pronounced in the austenitic regions.

3. The austenite matrix resulted in inducing better degree of abrasion resistance than the pearlite/bainite ones. In comparison with the pearlite/bainite, the austenite deformed more easily, delayed the fracture of the carbides, supported them, and transformed itself to form harder martensite during the abrasion process.

4. For all the samples investigated in this present study, the degree of hardness provided an excellent indication of the volume wear rate for the coated surfaces that contained high levels of chromium. As the overall hardness of the samples increased, the volume wear rate was recorded to decrease. In general, the wear rate of the samples constituting 20 wt.% Cr was approximately 3.5 times lower than that of the samples containing 10 wt.% Cr at an equivalent carbide volume fraction or an equivalent degree of hardness. In addition, the carbide volume fraction also provided an indication of the wear rate.

#### References

- [1] KULKARNI, K. M.—ANAND, V.: Metals Handbook. 9th ed. Metals Park, OH, ASM 1984.
- [2] KINZEL, A. B.—CRAFTS, W.: The Alloys of Iron and Chromium I. New York, McGraw-Hill 1937.
- [3] KINZEL, A. B.—FRANKS, R.: The Alloys of Iron and Chromium II. New York, McGraw-Hill 1937.
- [4] GUNDLACH, R. B.—PARKS, J. L.: *Wear*, **46**, 1978, p. 97. [doi:10.1016/0043-1648\(78\)90113-8](https://doi.org/10.1016/0043-1648(78)90113-8)
- [5] SU, Y. L.—SU, C. T.—YAO, S. H.—YUR, J. P.—HSU, C. A.—LIU, T. H.: *Vacuum*, **80**, 2006, p. 1021. [doi:10.1016/j.vacuum.2006.01.012](https://doi.org/10.1016/j.vacuum.2006.01.012)
- [6] KUMAR, K. S.—LAWLEY, A.—SANGAM, M.—STIEGLER, J. O.: High Temperature Alloys, Theory and Design. New York, AIME 1984.
- [7] LIANG, G. Y.—WONG, T. T.—MACALPINE, J. M. K.—SU, J. Y.: *Surface and Coatings Technology*, **127**, 2000, p. 232. [doi:10.1016/S0257-8972\(00\)00551-X](https://doi.org/10.1016/S0257-8972(00)00551-X)
- [8] PANG, W.—STODDART, P. R.—COMINS, J. D.—EVERY, A. G.—PIETERSEN, D.—MARAIS, P. J.: *Journal of Refractory Metals and Hard Materials*, **15**, 1997, p. 179. [doi:10.1016/S0263-4368\(96\)00037-6](https://doi.org/10.1016/S0263-4368(96)00037-6)
- [9] MATSUBARA, Y.—SASAGURI, N.—SHIMIZU, K.—YU, S. K.: *Wear*, **250**, 2001, p. 502. [doi:10.1016/S0043-1648\(01\)00599-3](https://doi.org/10.1016/S0043-1648(01)00599-3)
- [10] NAVAS, C.—CONDE, A.—FERNANDEZ, B. J.—ZUBIRI, F.—DAMBORENEA, J. D.: *Surface and Coatings Technology*, **19**, 2005, p. 136. [doi:10.1016/j.surfcoat.2004.05.002](https://doi.org/10.1016/j.surfcoat.2004.05.002)
- [11] OUYANG, J. H.—PEI, Y. T. T.—LEI, C.—ZHOU, Y.: *Wear*, **185**, 1995, p. 167. [doi:10.1016/0043-1648\(95\)06604-7](https://doi.org/10.1016/0043-1648(95)06604-7)
- [12] ACKER, K. V.—VANHOYWEGHEN, D.—PERSONS, R.—VANGRUNDERBEEK, J.: *Wear*, **258**, 2005, p. 194.
- [13] KUIRY, S. C.—WANNAPARHUN, S.—DAHOTRE, N. B.—SEAL, S.: *Scripta Materialia*, **50**, 2004, p.1237. [doi:10.1016/j.scriptamat.2004.02.005](https://doi.org/10.1016/j.scriptamat.2004.02.005)
- [14] YILMAZ, S. O.: *Surface and Coatings Technology*, **201**, 2006, p. 1568. [doi:10.1016/j.surfcoat.2006.02.038](https://doi.org/10.1016/j.surfcoat.2006.02.038)
- [15] YILMAZ, S. O.: *Surface and Coatings Technology*, **194**, 2005, p. 175. [doi:10.1016/j.surfcoat.2004.08.227](https://doi.org/10.1016/j.surfcoat.2004.08.227)
- [16] WANG, X. H.—SONG, S. L.—QU, S. Y.—ZOU, Z. D.: *Surface and Coatings Technology*, **201**, 2006, p. 5899. [doi:10.1016/j.surfcoat.2006.10.042](https://doi.org/10.1016/j.surfcoat.2006.10.042)
- [17] KORKUT, M. H.—YILMAZ, S. O.—BUYTOZ, S.: *Surface and Coatings Technology*, **157**, 2002, p. 5. [doi:10.1016/S0257-8972\(02\)00041-5](https://doi.org/10.1016/S0257-8972(02)00041-5)
- [18] MRIDHA, S.—ONG, H. S.—POH, L. S.—CHEANG, P.: *Journal of Material. Processing Technology*, **113**, 2001, p. 516. [doi:10.1016/S0924-0136\(01\)00609-4](https://doi.org/10.1016/S0924-0136(01)00609-4)
- [19] LIN, Y. C.—WANG, S. W.—WU, K. E.: *Surface and Coatings Technology*, **172**, 2003, p. 158. [doi:10.1016/S0257-8972\(03\)00389-X](https://doi.org/10.1016/S0257-8972(03)00389-X)
- [20] POWELL, G. L. F.: In.: *Proc. 35th Annual Conference of the Australian Institute of Metals*. Sydney, Australian Institute of Metals 1982, p. 57.
- [21] LAIRD, G.—GUNDLACH, R.—RÖHRIG, K.: *Abrasion-Resistant Cast Iron Handbook*. Des Plaines, Illinois, USA, AFS 2000.
- [22] ZUM GAHR, K. H.: *Tribology International*, **31**, 1998, p. 587. [doi:10.1016/S0301-679X\(98\)00079-6](https://doi.org/10.1016/S0301-679X(98)00079-6)
- [23] FULCHER, J. K.—KOSEL, T. H.—FIORE, N. F.: *Wear*, **84**, 1983, p. 313. [doi:10.1016/0043-1648\(83\)90272-7](https://doi.org/10.1016/0043-1648(83)90272-7)
- [24] GUNDLACH, R. B.—PARKS, J. L.: *Wear*, **146**, 1978, p. 97. [doi:10.1016/0043-1648\(78\)90113-8](https://doi.org/10.1016/0043-1648(78)90113-8)
- [25] JUNYI, S.—YUDING, J.—LUDEMA, K. C.: In: *Proc. Int. Conf. on Wear of Materials*. New York, ASME 1987, p. 661.
- [26] SU, J. Y.—ZHOU, Q. D.—JIA, Y. D.—LUDEMA, K. C.: In: *Proc. Int. Conf. on Wear of Materials*. New York, ASME 1987, p. 621.
- [27] TABRETT, C. P.—SARE, I. R.—GHOMASHCI, M. R.: *Int. Mater. Rev.*, **41**, 1996, p. 59.
- [28] JICHENG, Z.—ZHANPENG, J.: *Acta Metallurgica et Materialia*, **38**, 1990, p. 425. [doi:10.1016/0956-7151\(90\)90148-A](https://doi.org/10.1016/0956-7151(90)90148-A)
- [29] KOMVOPOULOS, K.: *Comptes Rendus Mécanique*, **336**, 2008, p. 149.
- [30] KOMVOPOULOS, K.: *Wear*, **200**, 1996, p. 305.
- [31] ZUM GAHR, K. H.: *Microstructure and Wear of Materials*. New York, ASME 1987.